JOURNAL OF AIRCRAFT
Vol. 44, No. 5, September–October 2007

Flight-Test Evaluation of a Helicopter Airborne Lidar

Naoki Matayoshi*
Japan Aerospace Exploration Agency, Mitaka, Tokyo 181-0015, Japan
Kimio Asaka†
Mitsubishi Electric Corporation, Amagasaki, Hyougo 661-8661, Japan
and
Yoshinori Okuno‡
Japan Aerospace Exploration Agency, Mitaka, Tokyo 181-0015, Japan

DOI: 10.2514/1.28338

The Japan Aerospace Exploration Agency has conducted ground and flight-test evaluations of a prototype 1.5-μm all-fiber pulsed coherent Doppler lidar produced by Mitsubishi Electric Corporation, which aims to measure three-axis components of airspeed and detect atmospheric turbulence ahead of a helicopter. In the ground test, the lidar has proven its capability to detect atmospheric turbulence with a scale of several tens of meters by accurately measuring helicopter rotor downwash. In the flight test, the lidar was installed in the Japan Aerospace Exploration Agency's MuPAL-ε research helicopter and the accuracy of real-time airspeed calculation using lidar outputs and the format of a real-time pilot display were evaluated. The lidar successfully measured three-axis airspeed components accurately even in low-airspeed flight regimes including hovering, backwards, and sideways flight where the conventional Pitôt-static system does not work and its capability as a helicopter airspeed sensor was proven. Some technical challenges were found for atmospheric turbulence detection, such as increasing the detection range and improving the data analysis and presentation. These results will be used to establish the specifications of practical airborne lidars.

I. Introduction

FOR helicopters, crosswinds encountered during hovering can be a serious hazard, resulting in crosswind speed limits being imposed on many helicopters. Despite this, helicopter pilots have no means to measure crosswind speed while hovering, because the conventional Pitôt-static system does not work at low airspeeds and only measures forward, not lateral, airspeed. A new airspeed sensor that measures lateral as well as longitudinal (and, if possible, vertical) airspeed components and covers entire flight envelopes is therefore strongly desired. The main difficulty of airspeed measurement at low airspeeds is that at such speeds the airflow around a helicopter is fully disturbed by the helicopter itself, mainly by the main rotor downwash.

A few low-airspeed sensors already exist, such as the omnidirectional airspeed sensor mainly used by military helicopters and the ultrasonic velocimeter developed by the Japan Aerospace Exploration Agency (JAXA) that measures three-axis true airspeed (TAS) components with high accuracy at a rate of 20 Hz [1]. However, the need to avoid the influence of main rotor downwash limits the locations at which it is possible to install such sensors to areas such as at the end of a long nose boom or at the top of the main rotor hub, and sensor calibration is complicated. These drawbacks make it difficult for these sensors to be widely applied to commercial helicopters.

In addition, helicopters occasionally encounter strong local atmospheric turbulence, especially when operating in mountainous areas or from rooftop helipads. If the wind field ahead of the aircraft can be detected and hazardous area information provided to pilots, flight safety should be greatly improved.

To satisfy these two requirements, airspeed measurement and detection of the wind field ahead of the aircraft, much research has been conducted in recent years into the development of new onboard airspeed sensors using Doppler lidar (light detection and ranging) technology. By measuring the Doppler shift of light backscattered by aerosols, a Doppler lidar can directly measure the motion of air masses far from the helicopter and free from the disturbance of the helicopter itself. These properties allow the measurement of airspeed even in the low-airspeed region of the flight envelope, eliminate the need for calibration, and afford greater freedom of sensor location.

During the 1980–90s, several airborne Doppler lidars were developed, which used laser diode pumped solid-state laser as a laser source [2–5]. However, their size and weight were too large to be installed practically in helicopters and the production costs were not affordable. As an alternative, all-fiber airborne Doppler lidars, which use an optical fiber laser source and amplifier, have been developed over the past few years. The all-fiber Doppler lidar has the following merits that make it suitable for helicopters: 1) small size and light weight by use of optical fiber laser source and amplifier; 2) high installation flexibility, because the laser transceiver and its optics may be separated and are connected using a flexible optical fiber linkage; 3) safety, by adopting an eye-safe 1.5-μm wavelength laser; 4) low cost and high reliability, by using optical components originally developed for optical fiber communications. Thales Avionics and ONERA have been developing a demonstrator of an airborne all-fiber continuous-wave (CW) coherent Doppler lidar (CDL) called DALHEC to measure three-axis TAS components, and have conducted helicopter flight tests [6,7]. JAXA has been developing an airborne all-fiber pulsed CDL with Mitsubishi Electric Corporation (MELCO) to detect clear air turbulence (CAT) at high altitudes where jet transports cruise [8]. Compared to a CW-CDL, a pulsed CDL has the great advantage of being able to measure air mass motions at many ranges simultaneously and so can be used as a wind measurement sensor that detects wind shear or atmospheric turbulence ahead of an aircraft as well as a TAS sensor. A number of technical challenges still remain to be overcome before pulsed CDL can be applied as a CAT sensor for jet transports, such as increasing the detection range and improving the signal-to-noise ratio (SNR) in

Presented as Paper 6117 at the AIAA Atmospheric Flight Mechanics Conference, San Francisco, 15–18 August 2005; received 26 October 2006; revision received 28 January 2007; accepted for publication 3 February 2007.

*Researcher, Operation and Safety Technology Team; matayoshi.naki@jaxa.jp. Member AIAA.
†Engineer, Communication Systems Center; Asaka.Kimio@ap.MitsubishiElectric.co.jp
‡Senior Researcher, Operation and Safety Technology Team; okuno.yoshinori@jaxa.jp. Member AIAA.

Fig. 1 JAXA's research helicopter MuPAL-ε.

high altitudes, that is, in low aerosol density environments. However, these difficulties are alleviated in helicopter applications, because helicopters fly at much lower speeds and altitudes than jet transports.

Here, the following two applications of a helicopter airborne lidar are considered:

Type 1: TAS measurement in low-airspeed regions. The type 1 lidar will measure two- or three-axis TAS components over the entire helicopter flight envelope, including the hover. A detection range of several tens of meters is adequate to avoid the disturbance of the helicopter itself, and there is just single detection point. Such a lidar can be realized with current-level technology.

Type 2: Measurement of small-scale atmospheric turbulence. The type 2 lidar will measure small-scale atmospheric turbulence ahead of the helicopter, such as is likely to exist in mountainous area and around high-rise buildings. To realize this, a number of technical problems remain to be overcome, such as enhancing the lidar to measure wind speeds at multiple points over a short time interval, and the development of a method to analyze the wind data in real time and a display format to present it to the pilot.

To demonstrate the feasibility of the helicopter airborne lidar and collect basic data to establish the types 1 and 2 lidar specifications, a flight-test evaluation of a MELCO all-fiber pulsed CDL prototype has been conducted by JAXA and MELCO using JAXA's research helicopter MuPAL-ε [9] (Fig. 1). A real-time TAS calculation method for the type 1 lidar and a pilot display format for the type 2 lidar were developed and evaluated by flight test. Helicopter downwash measurement simulating small-scale atmospheric turbulence was also carried out in a ground test.

II. Lidar System

A. System Configuration

The MELCO's lidar system used for the current evaluation is a 1.5-μm all-fiber pulsed CDL originally designed for ground use. The system's appearance, block diagram, and major specifications are shown in Figs. 2 and 3 and Table 1, respectively. Compared to JAXA's CAT detection lidar [8], the signal-processing function has been improved so that the device can output the velocity and SNR at each target range to other computers in real time. Doppler spectra of wind velocities at various target ranges are obtained in real time by signal processing of the digitized received signal using fast Fourier transform (FFT) and incoherent integration. However, the following two functions of the CAT detection lidar have not been implemented because the system was not originally designed for airborne applications:

1) Superheterodyne intermediate frequency control: The superheterodyne intermediate frequency of the receiver is fixed at zero so that the velocity measurement range is fixed at ± 38 m/s. For airborne use, it is desirable to vary the intermediate frequency according to the aircraft's airspeed to increase the velocity measurement range with limited receiver bandwidth.

2) Automatic polarization control: The polarization of received light is not controlled in this system. The polarization of received light carried by the optical fiber connecting the transceiver optics with the laser transceiver can be influenced by aircraft vibration and changes in ambient temperature. The resulting fluctuations in polarization may degrade the heterodyne detection efficiency.

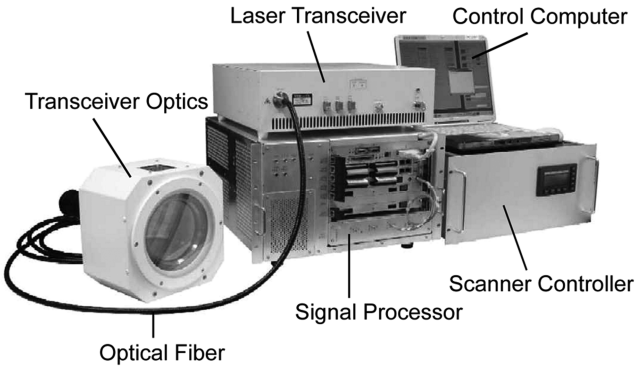

Fig. 2 Appearance of lidar.

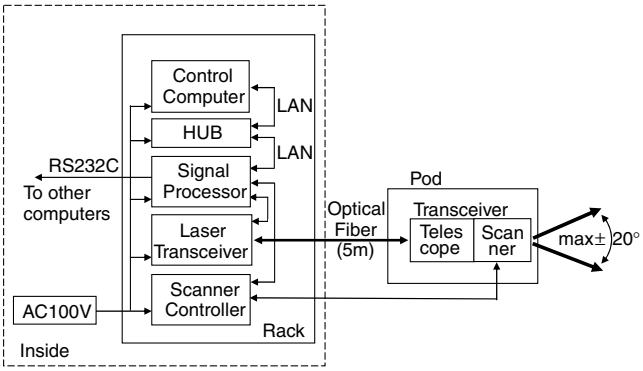

Fig. 3 Block diagram of lidar.

B. System Settings

To measure small-scale atmospheric turbulence, the pulse width was set to 0.2 μ sec, giving a range resolution of 30.7 m. Ten range bins were used so that the observation range was 45–322 m. The focus of the transceiver optics was adjusted to maximize the SNR at ranges of 150–200 m, which is almost the shortest focal setting of this system, to obtain stable wind data near the aircraft for TAS calculation. The number of incoherent integrations was set to 1000 or 4000 to increase the SNR, which gave data rates of four lines of sight (LOS)/ sec or 1 LOS/ sec, respectively. As to velocity range, both range ends of $\pm$35–38 m/s were not used to avoid FFT folding errors, resulting in a maximum velocity range of around $\pm$35 m/s.

Figure 4 shows ground test results that compare the lidar output with the ultrasonic anemometers outputs. Five ultrasonic anemometers were located along the lidar's LOS to produce reference wind

Table 1 Major lidar specifications

Items	Specification
Transmitted beam	Pulsed
Wavelength	1.5 μm
Pulse width	0.2 μ sec /0.5 μ sec
Pulse repetition frequency	4 kHz
Transmitted power (average)	$\leq$ 0.01 W (pulse width 0.2 μ sec)
	$\leq$ 0.02 W (pulse width 0.5 μ sec)
Velocity range	Max. $\pm$38 m/s
Velocity resolution	0.5 m/s or less
Observation range	Max. 2000 m (pulse width 0.5 μ sec)
Clear aperture of optics	100 mmϕ
Scan modes	Fixed, RHI, conical
Scan angle	Max. $\pm$20 deg

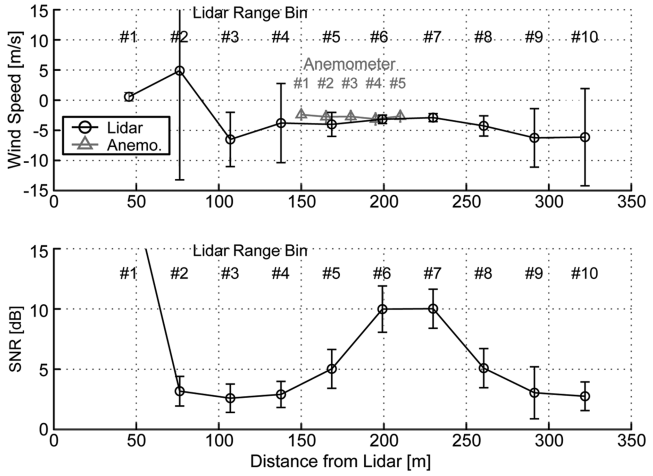

Fig. 4 Ground test results.

data. The upper graph shows the one-minute mean wind speeds and standard deviations of the lidar and the anemometers and the lower graph shows the SNRs of the lidar with 1000 incoherent integrations. Note that SNRs shown in this paper include the detectability improvement effects of incoherent integration. The SNR is defined as a product of signal-to-noise ratio and the square root of the number of integration. Because the lidar mainly receives internally reflected light in range bin no. 1, the SNR of range bin no. 1 is quite high and its velocity output is 0 m/s, not the real wind speed. The SNRs are relatively high for range bins nos. 5–8, which correspond to the configuration of the lidar optics. The velocity outputs of these range bins are therefore thought to be reliable, and showed good correspondence with the anemometer outputs. A SNR of 5 dB should be considered as a threshold for reliable velocity output.

III. Lidar Installation on Helicopter

For the flight test, the lidar was installed in the MuPAL-ε helicopter using existing hard points to reduce aircraft modification time and cost. A pod containing the transceiver optics was installed below the nose (Fig. 5a) using an existing nose-boom mount normally used to attach airdata sensors (Fig. 1). Because the transceiver optics contains moving parts and was not designed for airborne use, wire-rope type vibration absorbers were used to attenuate helicopter vibrations, resulting in a large pod size. Other lidar apparatus were mounted in a single rack installed in the cabin in place of a passenger seat (Fig. 5b).

IV. TAS Calculation Method

Conical scan patterns with an off-zenith angle of 15 or 20 deg were used, and the obtained data were used to calculate three-axis TAS components in real time (Fig. 6). The scan speed was set to 30 deg/s so that at least 12 LOS data would be obtained from each complete scan with 4000 incoherent integrations to produce accurate airspeed data. Two different calculation methods were applied; one using only the lidar's LOS data, and the other using inertial data to correct the lidar's LOS data for helicopter motion to improve the TAS calculation accuracy.

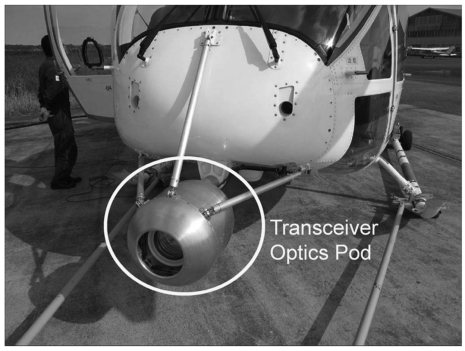

a) Transceiver optics pod

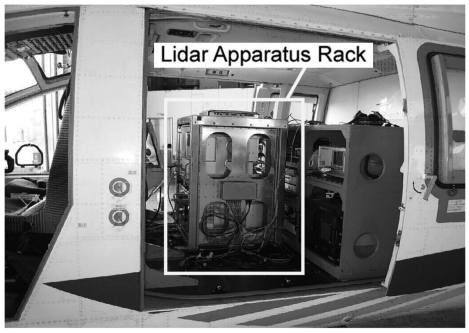

b) Apparatus rack

Fig. 5 Lidar installation on MuPAL-ε helicopter.

A. Using Lidar Data Only

Three-axis TAS components Vax_o^B, Vay_o^B, and Vaz_o^B in aircraft body axes at the lidar optics pod location were calculated by least-squares fitting the lidar velocity outputs v_i^{LOS} of a whole scan assuming that TAS and wind speed are constant spatially and temporally during a single scan. Here a "single scan" means the most recent complete revolution of the laser beam. This procedure is expressed in the following equations. The evaluation function f of the least-squares fitting is expressed as follows:

$$\frac{\partial f}{\partial Vax_o^B} = \frac{\partial f}{\partial Vay_o^B} = \frac{\partial f}{\partial Vaz_o^B} = 0$$

$$f = \sum_i \Big(Vax_o^B \cos\theta_i^B \cos\psi_i^B + Vay_o^B \cos\theta_i^B \sin\psi_i^B - Vaz_o^B \sin\theta_i^B - v_i^{\mathrm{LOS}} \Big)^2 \tag{1}$$

where the subscript i denotes each LOS data sample during a single scan. θ_i^B and ψ_i^B are the Euler angles that express the lidar's LOS direction relative to aircraft body axes and are calculated as follows:

$$\theta_i^B = \sin^{-1}\left(\frac{Lz_i^B}{\left(Lx_i^{B2} + Ly_i^{B2} + Lz_i^{B2} \right)^{1/2}} \right), \qquad \psi_i^B = \tan^{-1}\left(Lx_i^B / Ly_i^B \right), \qquad \begin{bmatrix} Lx_i^B \\ Ly_i^B \\ Lz_i^B \end{bmatrix} = \mathbf{E}(\Phi_R, \Theta_R, \Psi_R) \begin{bmatrix} \cos\alpha_i^L \\ \sin\beta_i^L \sin\alpha_i^L \\ -\cos\beta_i^L \sin\alpha_i^L \end{bmatrix}$$

$$\mathbf{E}(\phi, \theta, \psi) = \begin{bmatrix} \cos\theta\cos\psi & \sin\phi\sin\theta\cos\psi - \cos\phi\sin\psi & \cos\phi\sin\theta\cos\psi + \sin\phi\sin\psi \\ \cos\theta\sin\psi & \sin\phi\sin\theta\sin\psi + \cos\phi\cos\psi & \cos\phi\sin\theta\sin\psi - \sin\phi\cos\psi \\ -\sin\theta & \sin\phi\cos\theta & \cos\phi\cos\theta \end{bmatrix}$$

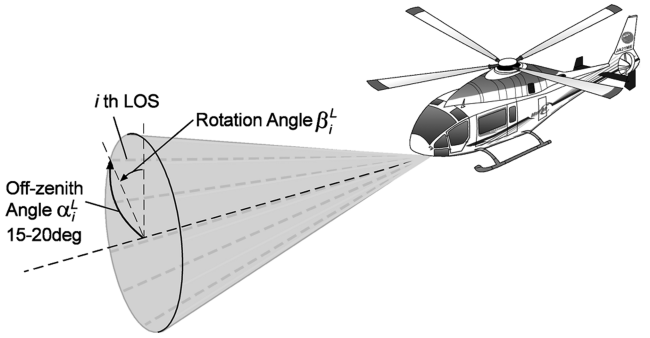

Fig. 6 Conical scan for TAS/wind calculation.

where α_i^L and β_i^L are the lidar's LOS off-zenith angle and rotation angle, respectively, relative to lidar-fixed axes (Fig. 6). Φ_R, Θ_R, and Ψ_R are the Euler angles that express the orientation of the lidar-fixed axes relative to aircraft body axes. By numerically solving these equations, three-axis TAS components in aircraft body axes are obtained.

B. Using Both Lidar and IMU Data (Aircraft Motion Compensation)

The TAS calculation error may increase during rapid aircraft maneuvers because TAS may change significantly during the 12-s scan period. To reduce this error, attitude and ground speed data from MuPAL-ε's onboard inertial measurement unit (IMU) were used in the TAS calculation to compensate aircraft motion. This IMU is internally coupled with a Differential Global Positioning System (DGPS) receiver and its major specifications are listed in Table 2. Compared to the lidar velocity resolution of 0.5 m/s (Table. 1), the IMU accuracy is adequately good so that its measurement errors are negligible for the TAS calculation. In this method of coupling the lidar with the IMU, three-axis wind speed components Wx^E, Wy^E, and Wz^E in Earth-fixed axes are calculated using the lidar velocity outputs and the IMU attitude/ground speed outputs assuming that only wind speed is constant spatially and temporally during a single scan. This procedure is expressed in the following equations. The evaluation function f_c of the least-squares fitting is

$$f_c = \sum_i \Big[Wx^E \cos\theta_i^E \cos\psi_i^E + Wy^E \cos\theta_i^E \sin\psi_i^E - Wz^E \sin\theta_i^E - \left(Vgx_{oi}^{\mathrm{LOS}} - v_i^{\mathrm{LOS}} \right) \Big]^2 \tag{3}$$

where θ_i^E and ψ_i^E are the Euler angles that express the lidar's LOS direction relative to Earth-fixed axes and Vgx_{oi}^{LOS} is the aircraft ground speed component in the lidar's LOS direction at the lidar optics pod location. θ_i^E and ψ_i^E are calculated as follows:

$$\theta_i^E = \sin^{-1}\left(\frac{Lz_i^E}{\left(Lx_i^{E2} + Ly_i^{E2} + Lz_i^{E2} \right)^{1/2}} \right)$$
$$\psi_i^E = \tan^{-1}\left(Lx_i^E / Ly_i^E \right), \qquad \begin{bmatrix} Lx_i^E \\ Ly_i^E \\ Lz_i^E \end{bmatrix} = \mathbf{E}(\Phi_i, \Theta_i, \Psi_i) \begin{bmatrix} Lx_i^B \\ Ly_i^B \\ Lz_i^B \end{bmatrix} \tag{4}$$

where Φ_i, Θ_i, and Ψ_i are the Euler angles that express the aircraft's attitude relative to Earth-fixed axes, measured by the IMU. Vgx_{oi}^{LOS} is calculated as follows:

$$\begin{bmatrix} Vgx_{oi}^{\mathrm{LOS}} \\ Vgy_{oi}^{\mathrm{LOS}} \\ Vgz_{oi}^{\mathrm{LOS}} \end{bmatrix} = \mathbf{E}^{-1}(0, \theta_i^B, \psi_i^B) \begin{bmatrix} Vgx_{oi}^B \\ Vgy_{oi}^B \\ Vgz_{oi}^B \end{bmatrix},$$
$$\begin{bmatrix} Vgx_{oi}^B \\ Vgy_{oi}^B \\ Vgz_{oi}^B \end{bmatrix} = \begin{bmatrix} Vgx_{mi}^B \\ Vgy_{mi}^B \\ Vgz_{mi}^B \end{bmatrix} + \begin{bmatrix} P_i^B \\ Q_i^B \\ R_i^B \end{bmatrix} \times \begin{bmatrix} Px^B \\ Py^B \\ Pz^B \end{bmatrix} \tag{5}$$

where Vgx_{mi}^B, Vgy_{mi}^B, and Vgz_{mi}^B are the aircraft ground-speed components in aircraft body axes at the IMU location and P_i^B, Q_i^B, and R_i^B are the aircraft angular velocities. Px^B, Py^B, and Pz^B are three-axis components of the position vector from the IMU location to the lidar optics pod location in aircraft body axes.

By numerically solving these equations, three-axis wind speed components in Earth-fixed axes are obtained. Three-axis TAS components Vax_{mi}^B, Vay_{mi}^B, and Vaz_{mi}^B in aircraft body axes at the IMU location are obtained using the obtained wind speed and the IMU-measured aircraft ground speed as follows:

$$\begin{bmatrix} Vax_{mi}^B \\ Vay_{mi}^B \\ Vaz_{mi}^B \end{bmatrix} = \begin{bmatrix} Vgx_{mi}^B \\ Vgy_{mi}^B \\ Vgz_{mi}^B \end{bmatrix} - \mathbf{E}^{-1}(\Phi_i, \Theta_i, \Psi_i) \begin{bmatrix} Wx^E \\ Wy^E \\ Wz^E \end{bmatrix} \tag{6}$$

V. TAS Calculation Results

Table 3 shows the lidar evaluation test cases including both ground and flight tests. Figure numbers are shown for the cases whose results are listed in this paper. Because of schedule constraints, only four flights were dedicated to lidar evaluation. Low-airspeed maneuvers such as hovering, hover turn, and forward–backward/sideways flights were conducted during the first two flights. High-airspeed maneuvers such as fast forward flight, steady sideslip, and ascent/descent were conducted during the latter two flights.

A. In-Flight Lidar SNR Output

In general, the lidar SNR outputs in flight tend to be lower than those on the ground because aerosol density becomes lower as altitude increases. In addition, the in-flight SNR of the evaluated lidar, which has no automatic polarization control, might be degraded due to the fluctuation of received light's polarization.

Figure 7 shows the in-flight lidar SNR outputs during flight nos. 3 and 4, which were flown at greater than 500 ft above the ground and so free from laser occlusion by the ground surface. Because the helicopter flew at relatively low altitudes of 1000–2000 ft, the in-flight SNRs are almost at the same level as, or are even better than, the

Table 2 MuPAL-ε onboard IMU specifications

Items	Accuracy	Rate
Pitch/roll	0.05 deg	50 Hz
Yaw	0.1 deg	50 Hz
Angular velocity	0.1 deg/s	50 Hz
Acceleration	0.098 m/s^2	50 Hz
Velocity[a]	0.1 m/s	50 Hz
Position[a]	1.0 m (horizontal); 2.0 m (vertical)	50 Hz

[a]DGPS hybrid

Table 3 Lidar evaluation cases

Flight	Aerosol density[a]	Test case (figure number)
Ground test	4×10^3	Functional check (Fig. 4) Hovering (Fig. 10) Low pass (Fig. 11)
No. 1	2×10^3	Hovering Hover turn Forward–backward (Fig. 8c) Sideways (Fig. 8d)
No. 2	2.5×10^3	Hovering (Fig. 8a) Hover turn (Fig. 8b) Forward–backward Sideways
No. 3	2.5×10^3	Wind measurement Level flight (Fig. 8e) Sideslip (Fig. 8f) Ascent/descent (Fig. 8g)
No. 4	12×10^3	Wind measurement Level flight (Fig. 8h) Sideslip Ascent/descent

[a]Number of aerosol particles larger than 0.3 μm in 47 ml atmosphere. Measured by a laser particle counter "Met One 227B."

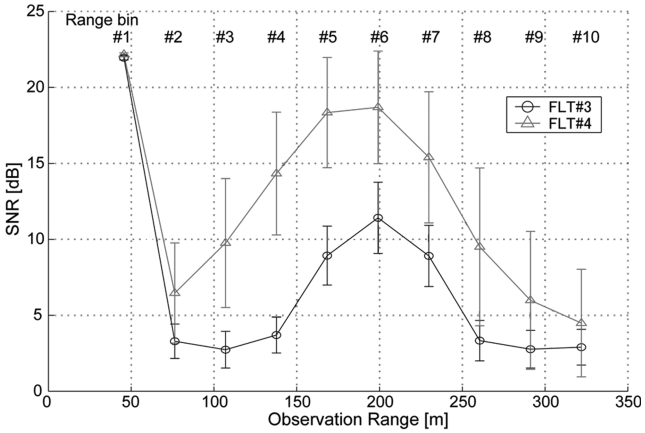

Fig. 7 Lidar SNR outputs during flight tests.

ground tests (Fig. 4), and no significant influence of polarization fluctuation is observed. The difference between the two flight results is thought to be mainly due to differences in aerosol densities. The aerosol density during flight no. 4 was almost five times greater than that during flight no. 3, as shown in Table 3.

As with the ground test results, the SNRs are relatively high for range bins nos. 5–7, which corresponds to the lidar optics setting. In the following airspeed calculations, the output of range bin no. 6, 200 m ahead of aircraft, was used because its SNR was stably high enough to provide reliable velocity outputs. In principle, short-range data such as for range bin no. 2 (range 75 m) should be used for airspeed calculation because the wind field may change as range increases. However, flight-test results proved that the SNRs for such short ranges were too low to use, mainly due to the limitations of the lidar optics setting.

B. Airspeed Calculation Accuracy

1. Hovering

Figure 8a shows the flight-test results of the helicopter hovering at a height of about 80 ft with its nose pointing directly into the wind. The upper three graphs show the three-axis TAS components in the aircraft body-axis system. The solid, dotted, and dashed lines, respectively, show the lidar outputs with and without aircraft motion compensation, and reference data. The reference data were obtained by subtracting the ground wind speed measured by an anemometer sited 10 ft above the ground from the aircraft's ground speed measured by the onboard IMU. The lower two graphs show aircraft attitude. The difference between the lidar outputs (solid and dotted lines) and the reference data (dashed line) observed in X-axis component is thought to be mainly due to the difference between wind speed at the hovering height (80 ft) and at the height of the anemometer (10 ft). The lidar outputs coincide well with the reference data in the other axes.

2. Hover Turn

Figure 8b shows the results of a hover turn maneuver at a height of about 80 ft. Unlike the hover case, the error of the lidar output without motion compensation is significant during the hover turn as the airspeed changes rapidly. Note that the errors of Z-axis components of lidar output are greater than those of other axes, regardless of motion compensation. Near the ground, data from the lower half of the conical scan cannot be used because the ground surface blocks the laser beam. This leads to a lack of data for the Z-axis component calculation and results in the observed large error.

3. Forward–Backward and Sideways Flights

Figures 8c and 8d show the results of forward–backward and sideways flights at a height of about 80 ft. The motion-compensated lidar output matches the reference data well. However, the lidar output without motion compensation always lagged the aircraft's motion. Because the lidar uses the most recent 12 s of data, its output without compensation looks like low-pass filtered aircraft motion. Differences between the compensated lidar output and the reference data observed in the X-axis component for forward–backward flight and in the Y-axis component for sideways flight are thought to be mainly due to wind speed differences with height, as in the hover case.

4. Fast Forward Flight

Figure 8e shows the results of steady forward flight at an altitude of about 1500 ft. Because the maximum measurable velocity of the lidar is about 35 m/s, the pilot maintained an airspeed of around 30 m/s. To provide reference data, midair wind speeds were estimated before the evaluation by flying a wind measurement pattern and assumed to be constant during the evaluation. The aircraft was flown in different several directions and the average wind speed was calculated using aircraft ground speed data. In addition, X- and Z-axis TAS components measured by the aircraft's calibrated Pitôt-static system are shown for reference as dash-dotted lines. The lidar outputs well agree with reference data. Unlike the hover turn case, the errors of the Z-axis component are almost the same as those of the Y axis because the data of an entire scan can be used away from the ground.

5. Steady Sideslip and Ascent/Descent

Figures 8f and 8g show the results of steady sideslip and ascent/descent at an altitude of about 1500 ft. These maneuvers were conducted to produce large Y- and Z-axis airspeed components, which are difficult for the lidar to measure because these axes are almost normal to the LOS. The lidar outputs, especially with motion compensation, measured Y- and Z-axis aircraft airspeeds well, except in the sideslip case during the 100–140 s interval (Fig. 8f), during which time the lidar did not work because the aircraft's airspeed temporarily exceeded its measurable velocity range.

6. Example of Airspeed Calculation Error due to Wind Shear

The airspeed calculations assume that the wind speed is spatially and temporally constant during a single scan of the lidar. If this assumption does not hold, a large airspeed error may result. Figure 8h shows the results of steady forward flight. Z-axis components of the lidar outputs have a fairly large error of 5–10 m/s, which implies the existence of a vertical wind shear. The greatest height difference between detection points in a single scan is about 400 ft. If the horizontal wind speed varies within this 400 ft, the lidar measurement produces a false vertical wind indication.

C. Discussions

The overall accuracies of lidar airspeed calculation are as follows:

1) Without motion compensation: 1.5–2 m/s in the X axis and 3–4 m/s in the Y and Z axes.

2) With motion compensation: 1–1.5 m/s in the X axis and 1.5–2 m/s in the Y and Z axes.

These values are calculated using all four evaluation flights data. Note that reference data errors are also included in these values.

The main error sources of the airspeed calculation are airspeed or wind speed changes during a single lidar scan period. To reduce the effect of airspeed change, aircraft motion compensation or an improved scanner that enables faster LOS sweep rates are required. To reduce the effect of wind speed changes, lidar data for ranges of several tens of meters should be used for the airspeed calculation. In addition, the Z-axis accuracy is reduced near the ground due to laser occlusion. This may be avoided by pointing the LOS upward.

VI. Atmospheric Turbulence Measurement

To test detection of small-scale atmospheric turbulence, the lidar system was mounted on a ground test bench and measured the downwash from a helicopter hovering close to the ground simulating small-scale atmospheric turbulence. In addition, a real-time pilot display format that shows the wind field ahead of a helicopter was developed and pilot comments were collected by the flight test.

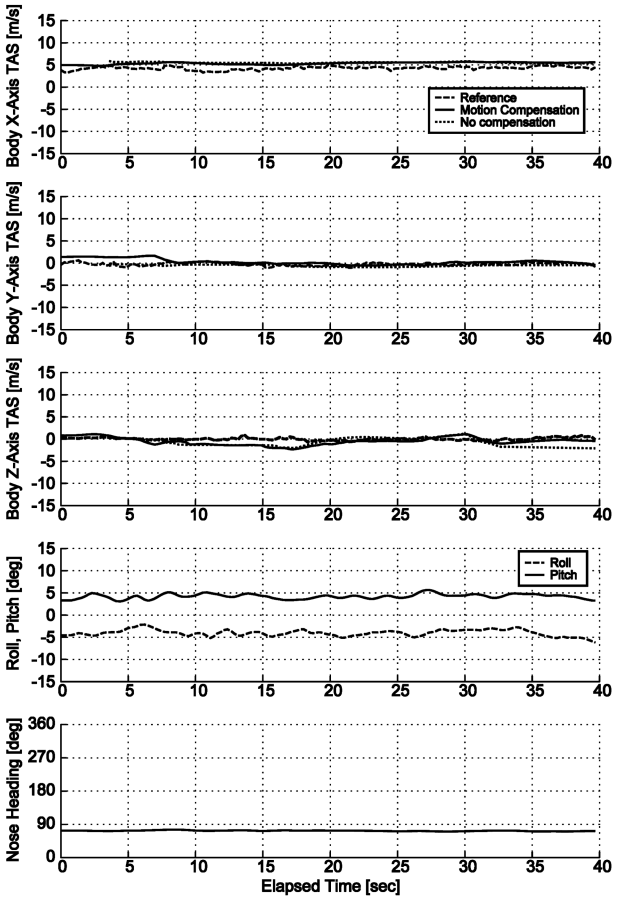

a) Hovering

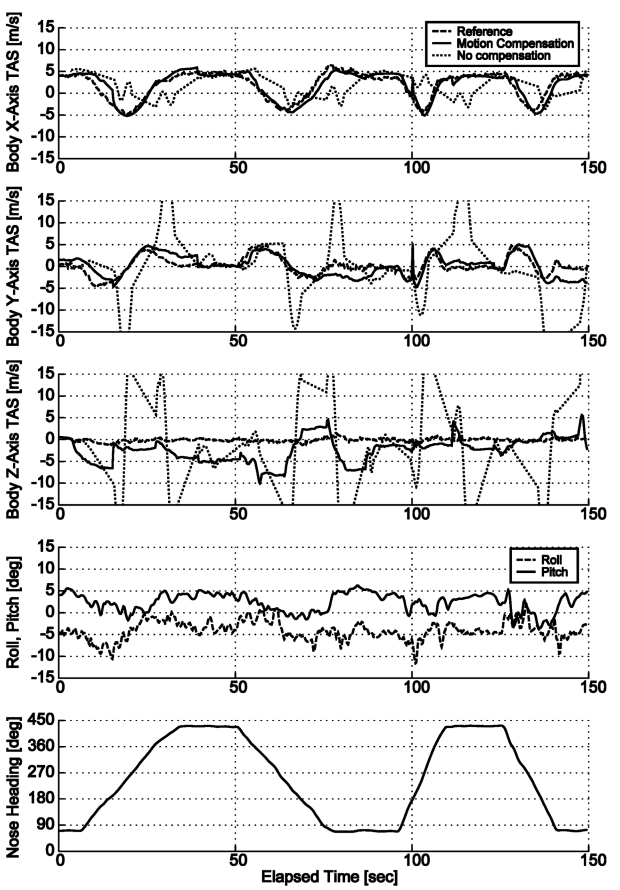

b) Hover turn

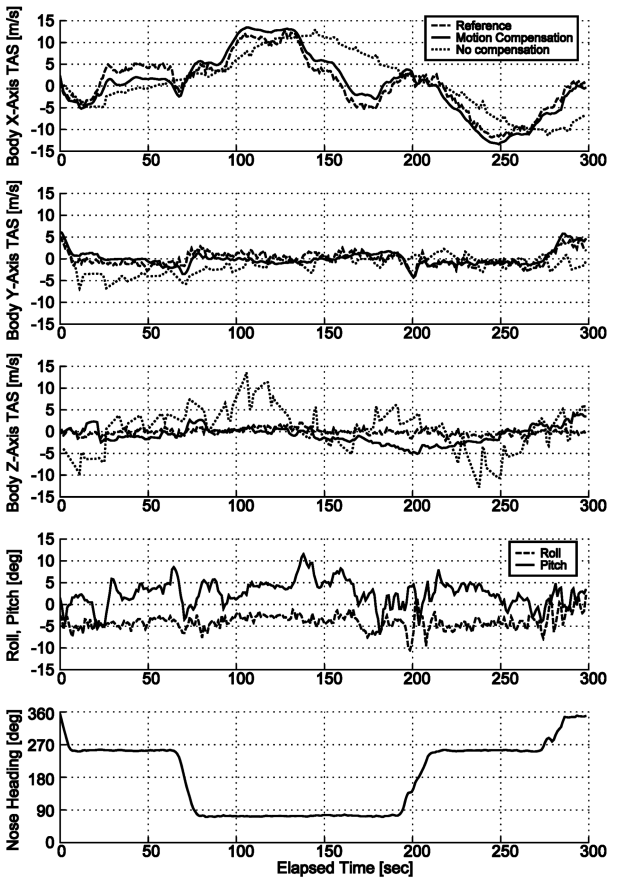

c) Forward-backward flight

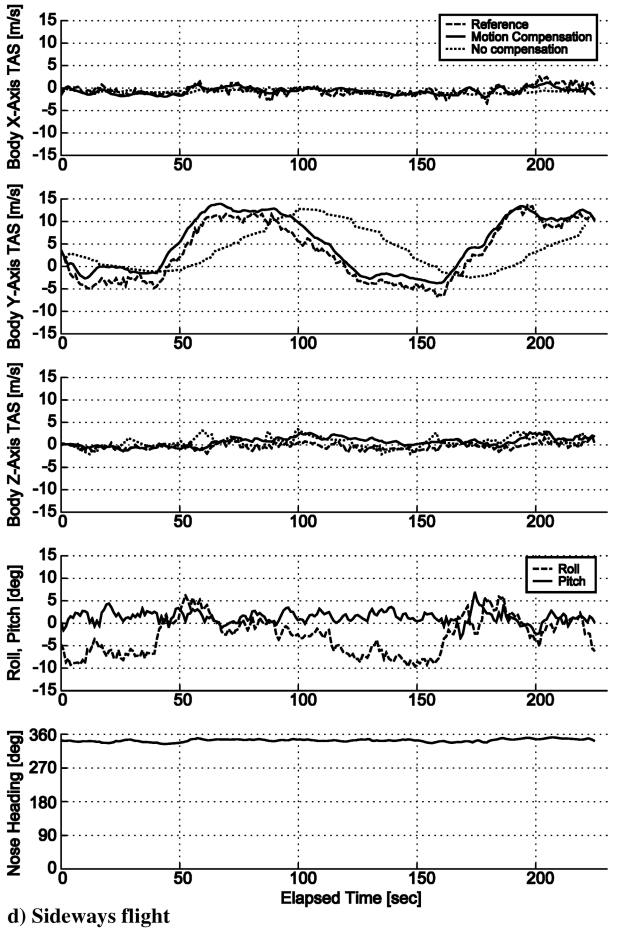

d) Sideways flight

Fig. 8 Airspeed calculation results.

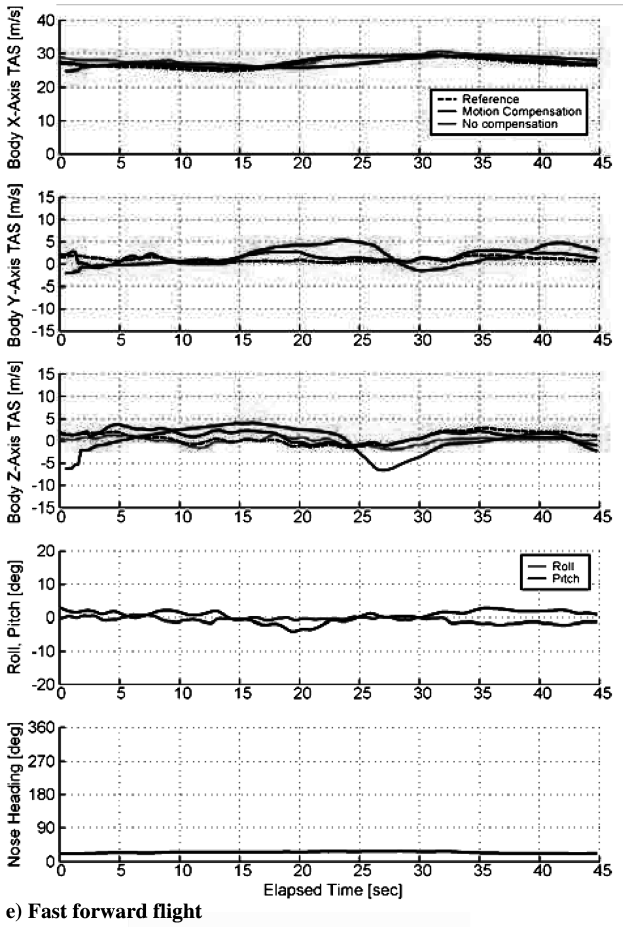

e) Fast forward flight

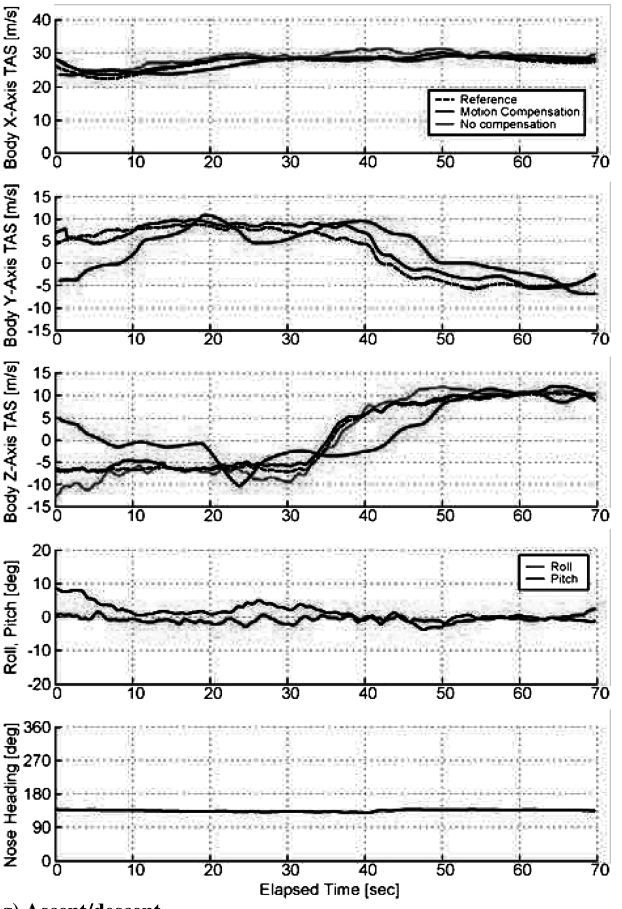

g) Ascent/descent

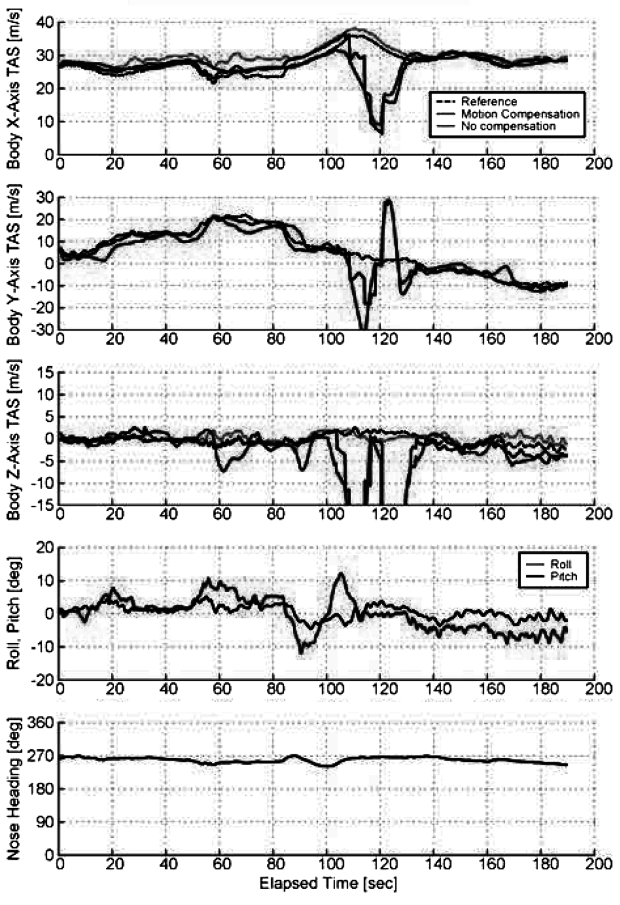

f) Steady sideslip

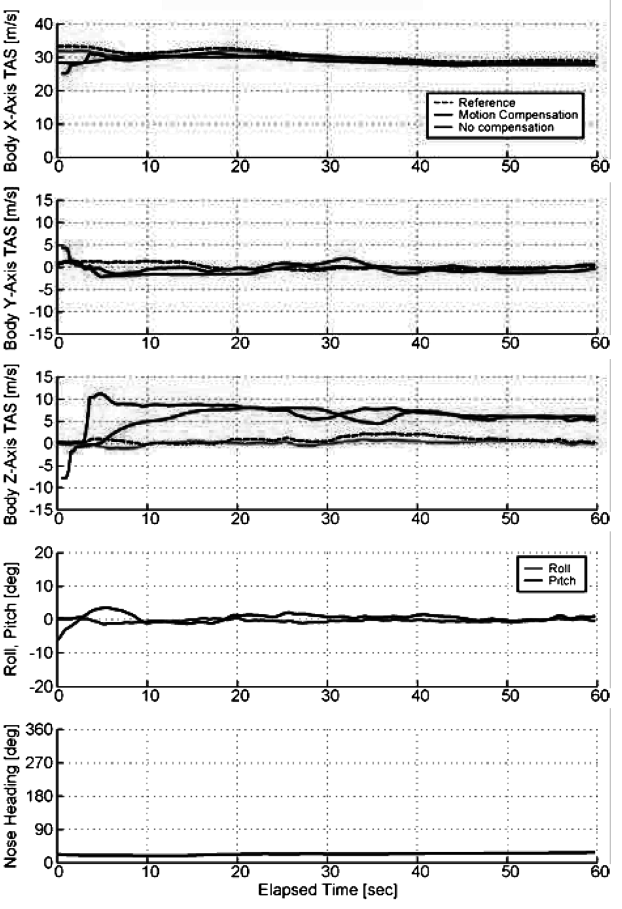

h) Example of airspeed calculation error

Fig. 8 Airspeed calculation results (continued).

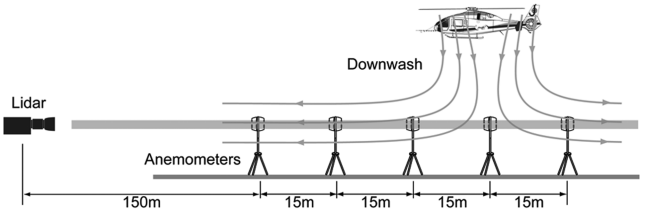

Fig. 9 Downwash measurement settings.

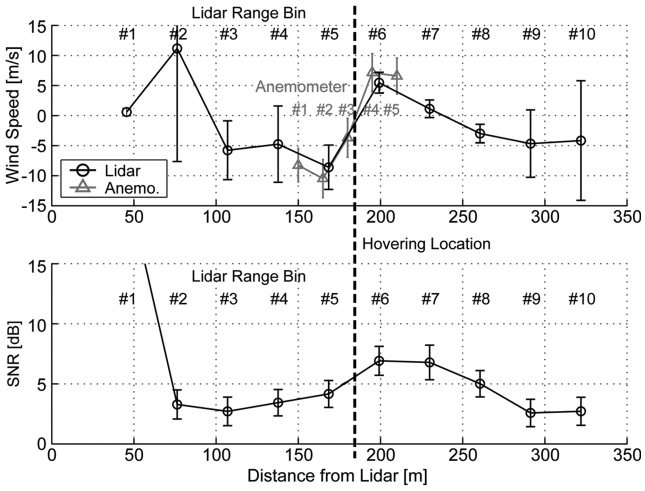

Fig. 10 Downwash measurement results (incoherent integration= 1000).

A. Helicopter Downwash Measurement

Figure 9 illustrates the downwash measurement setup. Five ultrasonic anemometers were located along the lidar's LOS to produce reference wind data. The distances between the lidar and the anemometers were 150–210 m, which corresponded to the lidar's optics and range settings. The MuPAL-ε helicopter hovered over the anemometers at a height of 60–80 ft while its position was recorded. Various wind fields were produced by changing the hover location.

Figure 10 shows downwash measurement results with the helicopter hovering 180 m from the lidar. The graph formats are the same as Fig. 4. The velocity outputs of range bin nos. 5–8, whose SNRs are relatively high, showed good correspondence with the anemometer outputs capturing downwash spreads. Figure 11 shows the velocity outputs of lidar range bin no. 6 (4 Hz output) and anemometer no. 4 (10 Hz output), which was located in the center of range bin no. 6, while the helicopter flew past over the anemometer. Although the wind field was fully turbulent and varied rapidly, the lidar output corresponds well with the anemometer output. Note that the fluctuation of the lidar output is smaller than that of the anemometer output because the lidar measures spatially averaged wind over a range bin length of 30 m and temporally averaged wind over a longer period of 0.25 s compared to the anemometer.

As the result of this ground test, the lidar's ability to detect small-scale atmospheric turbulence was proven.

B. Real-Time Display for Pilots

During flight-test evaluations, the helicopter's TAS and the wind field ahead of the helicopter were calculated in real time with aircraft motion compensation applied and displayed on a programmable display on the MuPAL-ε's instrument panel. Figure 12 shows a display image. A TAS indicator, which indicates horizontal TAS components with MuPAL-ε's 30 kt speed limits for backward and sideward flights, is shown in the lower right corner of the display, and three-axis components of wind speed are displayed at the upper left.

As to the wind field ahead of a helicopter, only LOS components of wind speeds are displayed in the horizontal/vertical section because the three-axis wind components calculation may be prone to large errors at long ranges as shown in Fig. 8h. In addition, low SNR data are not displayed to avoid false signals. LOS wind components are nearly identical to head/tail wind components because the lidar LOS is almost the parallel to the aircraft's X axis (Fig. 6). In the real-time display, head and tail wind components are displayed in blue and red, respectively.

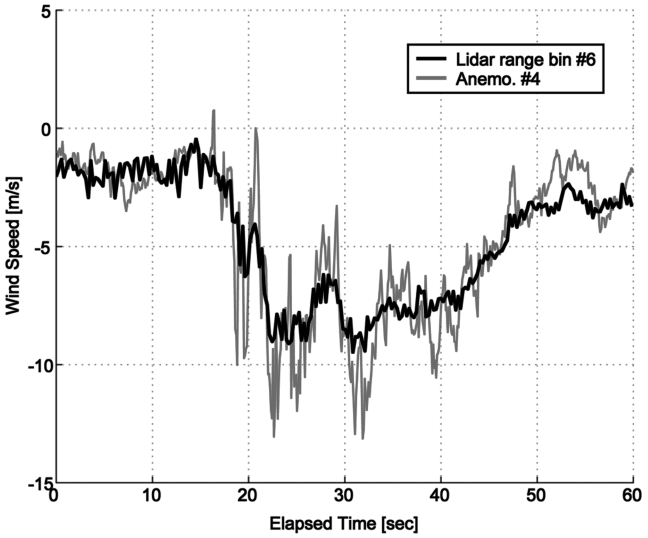

Fig. 11 Wind speed time histories of lidar and anemometer for turbulent wind case.

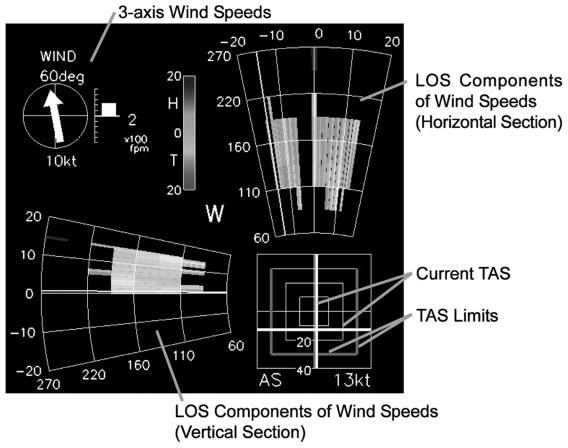

Fig. 12 Real-time display image.

C. Pilot Comments on the Real-Time Display

1. TAS Indicator and Wind Display

The motion-compensated lidar outputs are sufficiently accurate to be used for a TAS indicator and wind display, and its output rate of 1–4 Hz is also sufficient. However, the fluctuations of vertical airspeed indication are too large.

2. Display of Wind Situation Ahead of Aircraft

With the current display, which only shows observed wind speeds, it is difficult for a pilot to identify areas that may be hazardous to the safety of the aircraft. Any hazardous areas should be identified automatically and be displayed to the pilot directly. In addition, the current detection range of around 300 m is too short for a pilot to take action against atmospheric turbulence. A range of 1–2 km is necessary.

VII. Conclusions

The flight-test evaluation of a prototype lidar has proved its feasibility for helicopter applications. The results are summarized as follows:

1) The lidar system successfully measured three-axis TAS components accurately even during rapid maneuvering by compensating the aircraft's motions using onboard inertial data.

2) The lidar system has sufficient capability to detect small-scale atmospheric turbulence with a scale of several tens of meters, such as is likely to exist in mountainous areas or around high-rise buildings.

3) For type 1 lidar, which will measure three-axis TAS components, a quick LOS sweep rate, upward-pointing LOS and short-range detection capability are desirable. Furthermore, reducing the system's size, weight, and power consumption are the greatest technical challenges to realize a practical TAS measurement lidar.

4) For type 2 lidar, which will measure small-scale atmospheric turbulence ahead of an aircraft, optimization of the system for helicopter use, such as increasing the detection range to 1–2 km range with high range resolution, is necessary. This should be achieved by increasing the peak power of the emitted laser pulses and improving the signal detection efficiency. An intelligent data analysis algorithm that automatically identifies turbulence hazardous to flight from the measured wind data is also desirable for the real-time pilot display. To develop the data analysis algorithm, JAXA will use the results of its studies on the measurement of small-scale atmospheric turbulence and its influence on aircraft response using the MuPAL-ε helicopter and the ultrasonic velocimeter [10].

References

[1] Matayoshi, N., Inokuchi, H., Yazawa, K., and Okuno, Y., "Development of Airborne Ultrasonic Velocimeter and its Application to Helicopters," AIAA Paper 2005-6118, Aug. 2005.

[2] Targ, R., Steakley, B. C., Hawley, J. G., Ames, L. L., Forney, P., Swanson, D., Stone, R., Otto, R. G., Zarifis, V., Brockman, P., Calloway, R. S., Klein, S. H., and Robinson, P. A., "Coherent Lidar Airborne Wind Sensor 2: Flight-Test Results at 2 and 10 μm," *Applied Optics*, Vol. 35, No. 36, 1996, pp. 7117–7127.

[3] Hannon, S., and Thomson, J., "Aircraft Wake Vortex Detection and Measurement with Pulsed Solid-State Coherent Laser Radar," *Journal of Modern Optics*, Vol. 41, No. 11, 1994, pp. 2175–2196.

[4] Frehlich, R. G., Hannon, S. M., and Henderson, S. W., "Performance of a 2-micron Coherent Doppler Lidar for Wind Measurements," *Journal of Atmospheric and Oceanic Technology*, Vol. 11, No. 6, 1994, pp. 1517–1528.

[5] Hannon, S. M., Henderson, S. W., Thomson, J. A., and Gatt, P., "Autonomous Lidar Wind Field Sensor: Performance Predictions," *Proceedings of SPIE: The International Society for Optical Engineering*, Vol. 2832, 1996, pp. 76–91.

[6] Augere, B., and Cariou, J-P., "All-Fiber 1.5 μm CW Coherent Laser Anemometer for In-Flight Measurements," *Proceedings of SPIE: The International Society for Optical Engineering*, Vol. 5086, 2003, pp. 121–128.

[7] Cariou, J.-P., Augere, B., Goular, D., Schlotterbeck, J.-P., and Lacondamine, X., "All-Fiber 1.5 μm CW Coherent Laser Anemometer DALHEC—Helicopter Flight Test Analysis," *Proceedings of 13th Coherent Laser Radar Conference*, Tohoku Institute of Technology, Japan, Oct. 2005, pp. 157–160.

[8] Asaka, K., Fujiwara, T., Inagaki, T., Kameyama, S., Ando, T., Hirano, Y., and Harigae, M., "1.5 μm Airborne Coherent Doppler Lidar for CAT Sensor—Flight Test Results," *Proceedings of 13th Coherent Laser Radar Conference*, Tohoku Institute of Technology, Japan, Oct. 2005, pp. 153–156.

[9] Okuno, Y., and Matayoshi, N., "Development of a New Research Helicopter MuPAL-ε," *Proceedings of 57th Annual Forum*, Vol. 2, American Helicopter Society, Washington, DC, May 2001, pp. 2050–2058.

[10] Matayoshi, N., Okuno, Y., Maeyama, N., Zeng, P., Kose, Y., and Sato, H., "Measurement and Evaluation of Cliff-Top Turbulence Using a Research Helicopter," *Proceedings of the 30th European Rotorcraft Forum*, Association Aeronautique et Astronautique de France, France, Sept. 2004, pp. 184–188.